APSB
Acta Pharmaceutica Sinica B

2021
Vol.11   No.2
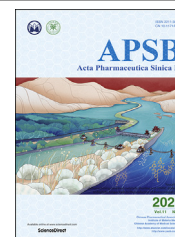
ORIGINAL ARTICLE

Development of hedgehog pathway inhibitors by epigenetically targeting GLI through BET bromodomain for the treatment of medulloblastoma

Xiaohua Liu[a,d,f,†], Yu Zhang[b,†], Yalei Li[c,†], Juan Wang[b],
Huaqian Ding[a,f], Wenjing Huang[b], Chunyong Ding[a,d],
Hongchun Liu[c,*], Wenfu Tan[b,*], Ao Zhang[a,d,e,f,g,*]

[a]CAS Key Laboratory of Receptor Research, Shanghai Institute of Materia Medica (SIMM), Chinese Academy of Sciences, Shanghai 201203, China
[b]Department of Pharmacology, School of Pharmacy, Fudan University, Shanghai 201203, China
[c]State Key Laboratory of Drug Research, Shanghai Institute of Materia Medica (SIMM), Chinese Academy of Sciences, Shanghai 201203, China
[d]School of Pharmacy, Shanghai Jiao Tong University, Shanghai 200240, China
[e]School of Life Science and Technology, ShanghaiTech University, Shanghai 201210, China
[f]University of Chinese Academy of Sciences, Beijing 100049, China
[g]State Key Laboratory of Esophageal Cancer Prevention and Treatment, Ministry of Education of China, Zhengzhou University, Zhengzhou 450001, China

Abstract   Medulloblastoma (MB) is a common yet highly heterogeneous childhood malignant brain tumor, however, clinically effective molecular targeted therapy is lacking. Modulation of hedgehog (HH) signaling by epigenetically targeting the transcriptional factors GLI through bromodomain-containing protein 4 (BRD4) has recently spurred new interest as potential treatment of HH-driven MB. Through

screening of current clinical BRD4 inhibitors for their inhibitory potency against glioma-associated onco-gene homolog (GLI) protein, the BRD4 inhibitor **2** was selected as the lead for further structural optimization, which led to the identification of compounds **25** and **35** as the high potency HH inhibitors. Mechanism profiling showed that both compounds suppressed HH signaling by interacting with the transcriptional factor GLI, and were equally potent against the clinical resistant mutants and the wild type of smoothened (SMO) receptor with IC_{50} values around 1 nmol/L. In the resistant MB allograft mice, compound **25** was well tolerated and markedly suppressed tumor growth at both 5 mg/kg (TGI = 83.3%) and 10 mg/kg (TGI = 87.6%) doses. Although further modification is needed to improve the pharmacokinetic (PK) parameters, compound **25** represents an efficacious lead compound of GLI inhibitors, possessing optimal safety and tolerance to fight against HH-driven MB.

1. Introduction

Medulloblastoma (MB) is one of the most common childhood malignant brain tumors[1,2], accounting for 6.6% of all pediatric central nervous system tumors (or 63.3% of all embryonal tumors) aging less than 19 years[3]. It is a small round blue cell tumor of the cerebellum with high heterogeneity, and biological characterization and molecular classification of MB remain as an unsettled challenge. Historically, MB is divided into four distinct molecular subgroups, namely: wingless (WNT), Sonic hedgehog (SHH), group 3 and group 4[4]. Among which, the SHH contains 30% of all MB diagnosis and is the most studied MB subgroup[5]. The SHH MB is characterized by the somatic mutations in the SHH pathway genes (Fig. 1), including the 12-pass transmembrane receptor patched (PTCH1), G protein-coupled receptor smoothened (SMO), and the downstream transcriptional factors GLI (GLI1, GLI2, and GLI3)[6,7]. In addition to MB, aberrant activations of SHH have also been observed in many other cancers, such as basal cell carcinoma (BCC)[8]. Currently, three SHH signaling pathway inhibitors (vismodegib[9,10],

sonidegib[11,12], and glasdegib[13], Fig. 1) have been approved as SMO antagonists for clinical use of locally advanced or metastatic BCC, or acute leukemia. Unfortunately, clinical trials of these compounds with MB patients have not yet met success due to their transient effects as well as SMO mutation-induced drug resistance during treatment[14−16]. Therefore, the standard treatment for MB after surgery remains to be craniospinal irradiation, chemotherapy or their combinations, which are associated with many adverse effects[17−19]. Although more precise molecular classification of MB and the genomic and epigenetic alterations have been recently reported[4], clinically effective treatment of MB remains to be an unmet medical need[20].

Since the transcriptional factor GLI is the final effector of the canonical HH signaling, acting downstream of SMO, inhibition of GLI function may overcome clinically observed drug resistance of SMO antagonist treatment[20−23]. Meanwhile, *Gli1* is the first identified HH pathway gene amplified in many HH-dependent cancers, and expression of *Gli1* is a reliable marker of HH pathway activity[20,24]. Therefore, development of GLI-targeting inhibitors has become an attractive strategy to treat MB and
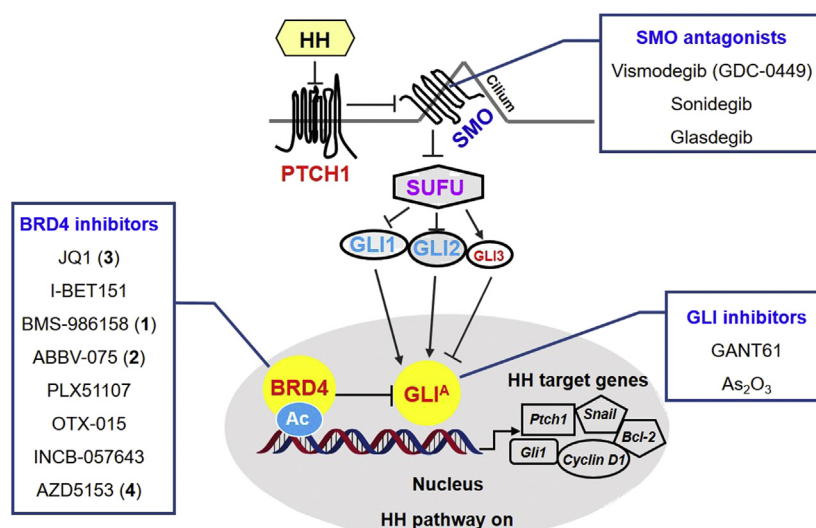

Figure 1 The hedgehog signaling pathway and representative inhibitors of SMO, GLI and BRD4. Ac, acetylation; BRD4, bromodomain-containing protein 4; GLI, glioma-associated oncogene homolog protein; GLI^A, activated GLI; HH, hedgehog; PTCH, patched; SMO, smoothened; SUFU, suppressor of fused.

many other cancers. Unfortunately, currently available GLI inhibitors such as GANT61[25,26] and As$_2$O$_3$[27] (Fig. 1) suffer from either toxicity or poor druglikeness or both.

Recently, modulation of HH signaling by epigenetically targeting GLI through bromodomain-containing protein 4 (BRD4) has spurred new interest in the development of effective treatment for HH-dependent tumors, especially for MB[28,29]. BRD4, together with BRD2, BRD3 and the testis-specific BRDT constitutes the important family of bromo and extra C-terminal (BET) bromodomain proteins, all containing two bromodomains BD1 and BD2 at the N terminus[30,31]. As a serine kinase of RNA Pol II and an atypical histone acetyltransferase, BRD4 recruits transcriptional regulatory complexes to acetylate chromatin *via* recognition of acetylated lysines[32]. Global mRNA expression profiling of clinical primary MB and normal cerebellar samples indicate that BRD2, BRD3, and BRD4 are all up-expressed in primary MB, especially SHH MB subgroups, whereas only marginal expression of BRD4 expressed in normal cerebellar tissues[33]. These results indicate that BRD4 together with BRD2 and BRD3 is involved in the pathogenesis of MB.

To decode the underlying mechanism of BRD4 involved in MB, Tang et al.[28] and Long et al.[29] recently disclosed that the bromodomains of BRD4 interact with GLI by occupying the cancer-specific proximal promoters of *Gli1* and *Gli2* genes. Notably, knockdown of *Brd4* did not abrogate GLI activity completely, and knockdown of either *Brd2* or *Brd3* also resulted in substantial GLI reduction, suggesting pan-BET inhibitors might be more efficacious than selective ones to modulate GLI[28]. Collectively, these pioneering studies provide the basis that inhibition of GLI can be achieved by suppression of BRD4, thus providing an alternative strategy for development of GLI inhibitors to treat HH-dependent MB. This strategy is especially appealing since development of highly potent GLI inhibitors is challenging due to the lack of targetable binding domains of GLI[20]. Therefore, in this report we first conducted a drug repurposing campaign by screening current clinically investigational BRD4 inhibitors bearing different chemotypes for their inhibitory potency against the HH pathway. The BRD4 inhibitor ABBV-075[34−38] is then selected as the lead for further structural optimization leading to identification of compounds **25** and **35** as

highly potent GLI inhibitors, especially compound **25** which was well tolerated and showed significant tumor growth inhibition in the resistant MB allograft mice. These results not only confirm the effectiveness of development of GLI inhibitors through optimization of BRD4 inhibitors, but also provide an alternative utility for BRD4 inhibitors in the treatment of many highly heterogeneous and untreatable pediatric brain tumors, such as MB[33,39,40].

2. Results and discussions

2.1. Chemistry

The synthesis of carbamates **5** and **6** is outlined in Scheme 1. Pd-catalyzed coupling of 3-amino-5-bromo-1-methylpyridin-2(1*H*)-one (**46**) with borate **47**[35] provided compound **48** in 84% yield, which was then subjected to aromatic substitution to give 2,4-difluorophenyl ether **49**. Substitution of **49** with ethyl carbonochloridate or 2-methoxyethyl carbonochloridate afforded corresponding carbamate **50a** or **50b** in 66%−71% yields. Subsequent reduction of **50a** or **50b** under iron powder followed by substitution with ethanesulfonyl chloride gave target compounds **5** and **6** in 54% and 70% yields, respectively.

The preparation of 3-aminopyridinones **7**−**11** was described in Scheme 2. Compounds **52a**−**e** were obtained from substitution reaction of aminopyridinone **46** or C−N coupling reaction of **51** with appropriate amines. Coupling of **52a**−**e** with borate **53**[41] under Pd(PPh$_3$)$_4$ catalysis yielded compounds **54a**−**e** in 59%−87% yields, which were readily converted to sulfonamides **7**−**11** by reacting with ethanesulfonyl chloride in the presence of Et$_3$N.

As shown in Scheme 3, substituted arylamine **55**, which was prepared[41] by following literature procedures, was reacted with sulfurisocyanatidic chloride followed by cyclization with 1,2-dibromoethane or 1,3-dibromopropane to deliver **56a** and **56b** in 90% and 88% yields, respectively. Subsequent reduction of the esteric moiety by NaBH$_4$ followed by *N*-Ts deprotection with NaOH afforded compounds **12** and **13** in 72% and 78% yields, respectively.

The synthesis of sulfuric diamides **14**−**23** is illustrated in Scheme 4. Sulfuric diamide **57** was generated from substitution reaction of **55** with freshly made *tert*-butyl(chlorosulfonyl)
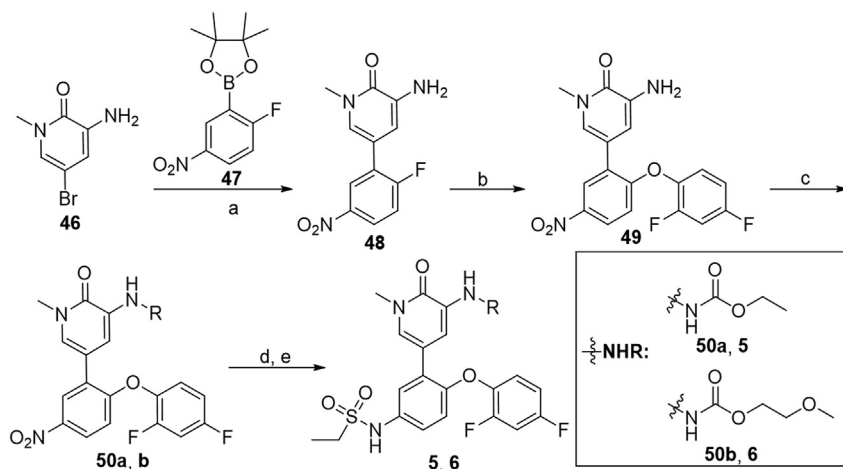
Scheme 1   Synthesis of compounds **5** and **6**. Reagents and conditions: (a) **47**, Pd(PPh$_3$)$_4$, 1,4-dioxane/2 mol/L Na$_2$CO$_3$ aq. (5:1), microwave 120 °C, 1 h, 84%; (b) 2,4-difluorophenol, Cs$_2$CO$_3$, DMF, r.t., 1 h; (c) ethyl carbonochloridate or 2-methoxyethyl carbonochloridate, NaH, THF, 0 °C to rt, 1 h, 66%−71%; (d) Fe, NH$_4$Cl, EtOH/H$_2$O (5:2), 70 °C, 3 h; (e) ethanesulfonyl chloride, pyridine, microwave 130 °C, 15 min, 54%−70%.

carbamate in 74% yield. Cyclization of compound **57** with 1,2-dibromoethane or 1,3-dibromopropane delivered 1,2,5-thiadiazolidine 1,1-dioxides **58a** and **58b** in 54% and 75% yields, respectively. *N*-Boc deprotection of **58a** or **58b** with TFA and further substitution with different alkyl bromides afforded compounds **59a−d** in 68%−98% yields. Subsequent *N*-Ts deprotection of compounds **59a−c** in the presence of NaOH afforded corresponding compounds **14**, **15** and **23** in 89%−93% overall yields. It should be noted that compounds **16−19** were prepared by *N*-Boc deprotection of **58b** with TFA, subsequent *N*-Ts deprotection and further substitution with 1,1-difluoro-2-iodoethane or different alkyl bromides in 28%−55% overall yields. In addition, substitution of bromide **59d** with different amines followed by *N*-Ts deprotection with NaOH delivered compounds **20−22** in 75%−78% yields.

As shown in Scheme 5, compounds **24** and **25** bearing the 3-fluoro-6-methyl-1,6-dihydro-7*H*-pyrrolo[2,3-*c*]pyridin-7-one scaffold were prepared. Starting from 4-fluoro-1*H*-pyrrole-2-carboxylic acid **60**[42], C-3 fluorinated bicyclic pyrrolopyridone core **62** was prepared in 68% overall yield by first condensation of **60** with 2,2-dimethoxyethanamine followed by self-cyclization in the presence of *p*-toluene sulfonic acid. Protection of pyrrolidine **62** with TsCl in the presence of NaH followed by bromination with NBS generated the intermediate **63** in 84% yield over two steps. Coupling of aryl bromide **63** with borate **53** under Pd(PPh$_3$)$_4$ catalysis afforded compound **64** in 85% yield. Treatment of compound **64** with 3-chloropropane-1-sulfonyl chloride or 4-chlorobutane-1-sulfonyl chloride yielded bis-substituted **65a** and **65b** in 64% and 68% yields, respectively. Subsequent *N*-Ts deprotection, *N*-sulfonyl removal and intramolecular cyclization of compounds **65a** and **65b** in one pot with NaOH afforded target compounds **24** and **25** in 95% and 91% yields, respectively.

As shown in Scheme 6, carboxylic acids **26** and **27** and amides **28−32** were obtained using 6-methyl-1-tosyl-1,6-dihydro-7*H*-pyrrolo[2,3-*c*]pyridin-7-one **66** as the starting material. Substitution of the pyrrole C-2 of **66** with ethyl chloroformate delivered ethyl ester **67**, which was then converted to compounds **68a** and **68b** through a similar reaction as that for **65a** and **65b**. Subsequent *N*-Ts deprotection, *N*-sulfonyl removal, intramolecular cyclization and ethyl ester hydrolysis were conducted in one pot in the presence of NaOH leading to acids **26** and **27** in 83% and 89% yields, respectively. Condensation of **26** or **27** with NH$_4$Cl, CH$_3$CH$_2$NH$_2$ or 3-(4-methylpiperazin-1-yl)propan-1-amine in the presence of HOBT, EDCI and Et$_3$N produced compounds **28−32** in 65%−78% yields.

Compounds **33−39** bearing benzofuran or cycloalkyl amine moieties were synthesized as described in Scheme 7. Aromatic substitution of compound **69**[34] with benzofuran-5-ol or different
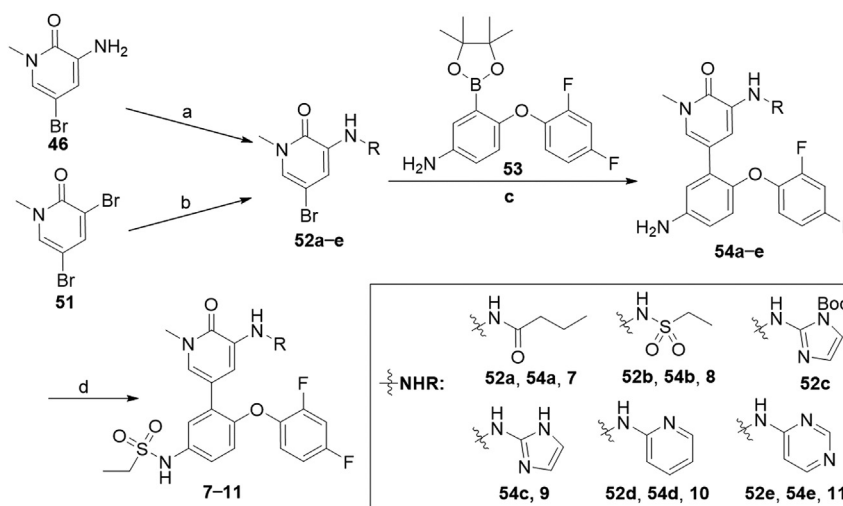
Scheme 2 Synthesis of compounds **7−11**. Reagents and conditions: (a) RH, Et$_3$N, DCM, r.t., 1 h; (b) RH, Pd$_2$(dba)$_3$, xantphos, Cs$_2$CO$_3$, toluene, 100 °C, 3 h, 19%−71%; (c) **10**, Pd(PPh$_3$)$_4$, 1,4-dioxane/2 mol/L Na$_2$CO$_3$ aq. (5:1), 100 °C, 1 h, 59%−87%; (d) i) ethanesulfonyl chloride, Et$_3$N, DCM, r.t., 1 h; ii) NaOH, 1,4-dioxane, 90 °C, 30 min, 33%−62%.
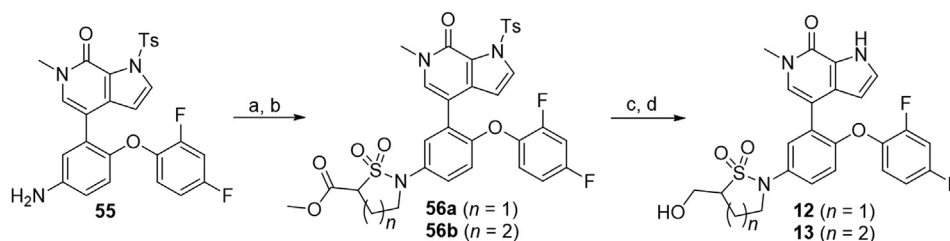
Scheme 3 Synthesis of compounds **12** and **13**. Reagents and conditions: (a) methyl 2-(chlorosulfonyl)acetate, Et$_3$N, DCM, r.t., 1 h, 88%; (b) 1,2-dibromoethane or 1-bromo-3-chloropropane, K$_2$CO$_3$, DMF, 70 °C, 88%−90%; (c) NaBH$_4$, CaCl$_2$, dry THF, 0 °C to r.t., 3 h; (d) NaOH, 1,4-dioxane, 90 °C, 30 min, 72%−78% over two steps.
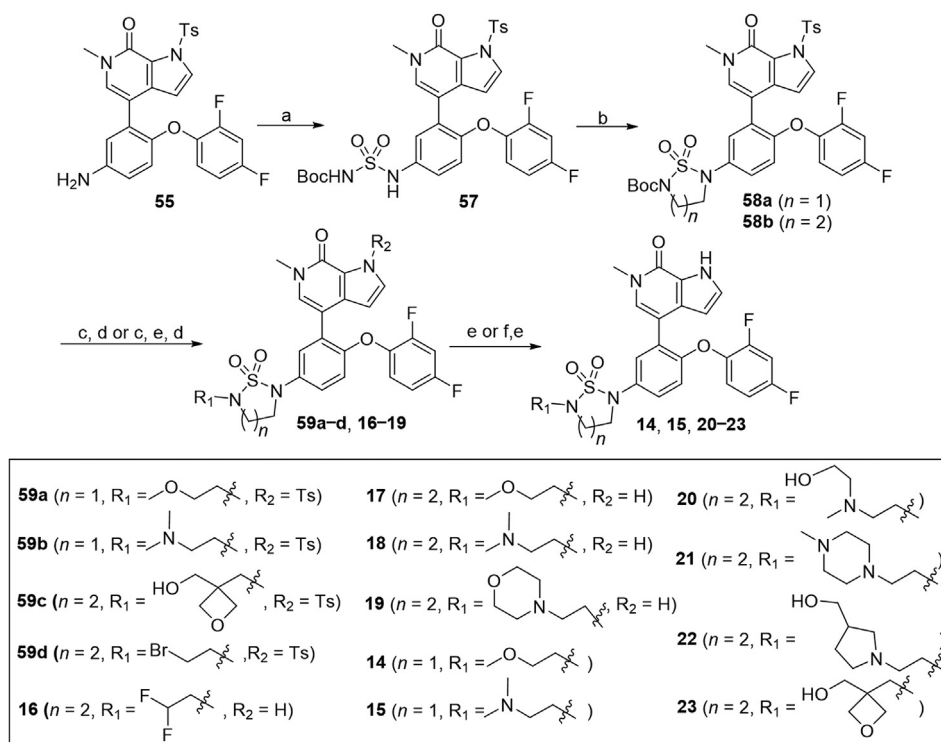
Scheme 4 Synthesis of compounds **14–23**. Reagents and conditions: (a) sulfurisocyanatidic chloride, *t*-BuOH, Et$_3$N, DCM, 0 °C to r.t., 2.5 h, 74%; (b) 1,2-dibromoethane or 1,3-dibromopropane, K$_2$CO$_3$, MeCN, reflux, overnight, 54%–75%; (c) TFA, DCM, r.t., 2 h; (d) RBr or (for **16**) RI, K$_2$CO$_3$, DMF, 60 °C, 1–5 h; (e) NaOH, 1,4-dioxane, 90 °C, 30 min; (f) from **59h**, amines, K$_2$CO$_3$, MeCN, 60 °C, 75%–78%.

amines furnished compounds **70a–e** in 33%–98% yields, which were then reduced by hydrogen atmosphere under Pd/C or by iron powder in the presence of NH$_4$Cl to afford corresponding anilines **71a–e**. It is worth noting that *N*-Ts protecting group was partially taken off during substitution reaction with *trans*-4-methylcyclohexyl amine. In this case, additional *N*-Ts protection under NaH was necessary to afford compound **70b**. Treatment of compounds **71a–e** with 3-chloropropane-1-sulfonyl chloride or 4-chlorobutane-1-sulfonyl chloride provided di-substituted

intermediate **72a** and mono-substituted **72b–g** in 34%–78% yields. It should be pointed out that for compound **71e**, the two hydroxyl groups need to be protected with TMSCl before treatment with 4-chlorobutane-1-sulfonyl chloride. Finally, N-deprotection, *N*-sulfonyl removal and intramolecular cyclization of compounds **72a–g** were conducted in one pot in the presence of NaOH to provide target compounds **33–39** in 85%–93% overall yields.

The synthesis of C-2 or C-3 fluorinated pyrropyridinones **40–45** bearing a 4-methylcyclohexan-1-amino motif was
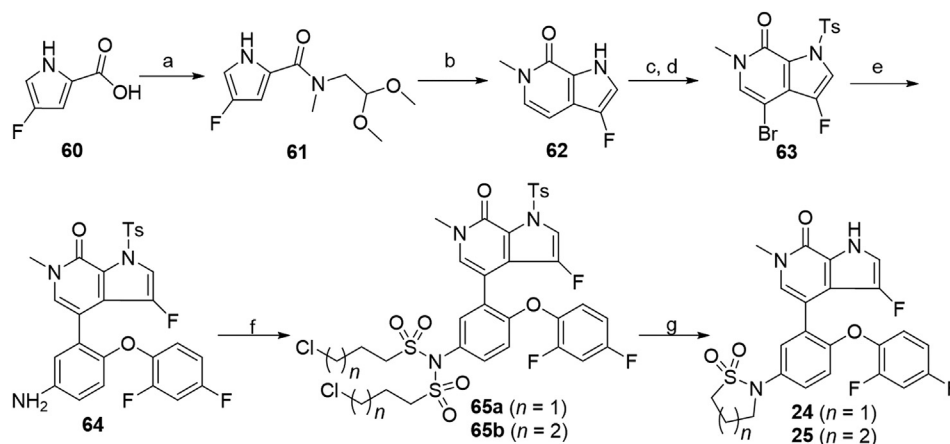
Scheme 5 Synthesis of compounds **24** and **25**. Reagents and conditions: (a) 2,2-dimethoxyethanamine, DIPEA, propanephosphonic acid cyclic anhydride, THF, −5–60 °C, 20 h, 75%; (b) TsOH·H$_2$O, THF, 60 °C, overnight, 90%; (c) TsCl, NaH, DMF, 0 °C, 1 h; (d) NBS, TsOH·H$_2$O, THF, r.t., 1 h, 84% over 2 steps; (e) **53**, Pd(PPh$_3$)$_4$, 1,4-dixone/2 mol/L Na$_2$CO$_3$ aq. (5:1), 100 °C, 1 h, 85%; (f) 3-chloropropane-1-sulfonyl chloride or 4-chlorobutane-1-sulfonyl chloride, Et$_3$N, DCM, r.t., 1 h, 64%–68%; (g) NaOH, 1,4-dioxane, 90 °C, 0.5 h, 91%–95%.
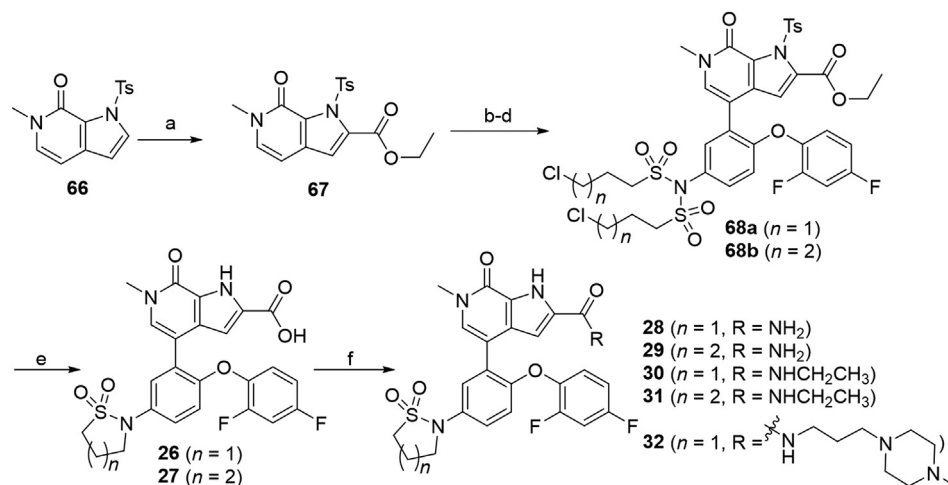
Scheme 6 Synthesis of compounds **26–32**. Reagents and conditions: (a) *n*-BuLi, ethyl carbonochloridate, dry THF, N₂, −10 °C, 1 h, 60%; (b) NBS, TsOH·H₂O, THF, r.t., 1 h; (c) **53**, Pd(PPh₃)₄, 1,4-dixone/2 mol/L Na₂CO₃ aq. (5:1), 100 °C, 1 h, 76%; (d) 3-chloropropane-1-sulfonyl chloride or 4-chlorobutane-1-sulfonyl chloride, Et₃N, DCM, r.t., 1 h, 84%–88%; (e) NaOH, 1,4-dioxane, 90 °C, 0.5 h, 89%–92%; (f) HOBT, EDCI, Et₃N, NH₄Cl or CH₃CH₂NH₂ or 3-(4-methylpiperazin-1-yl)propan-1-amine, DCM, r.t., 3 h, 65%–78%.

described in Scheme 8. Fluorination of pyrrole C-2 of **66** with NFSI under *n*-BuLi delivered compound **73** in 45% yield, which was brominated to yield intermediate **74** through a similar reaction as described in Scheme 5. Borate **77** was obtained in 80% overall yield with 1-fluoro-4-nitrobenzene (**75**) as the starting material by substitution with *trans*-4-methylcyclohexyl amine

followed by coupling with bis(pinacolato)diboron. The coupling of borate **77** with aryl bromide **63** or **74** delivered corresponding **78a** and **78b** in 57% and 68% yields, respectively, which were then converted to target compounds **40–45** in 65%–85% overall yields through a similar reaction procedure as described in Scheme 7.
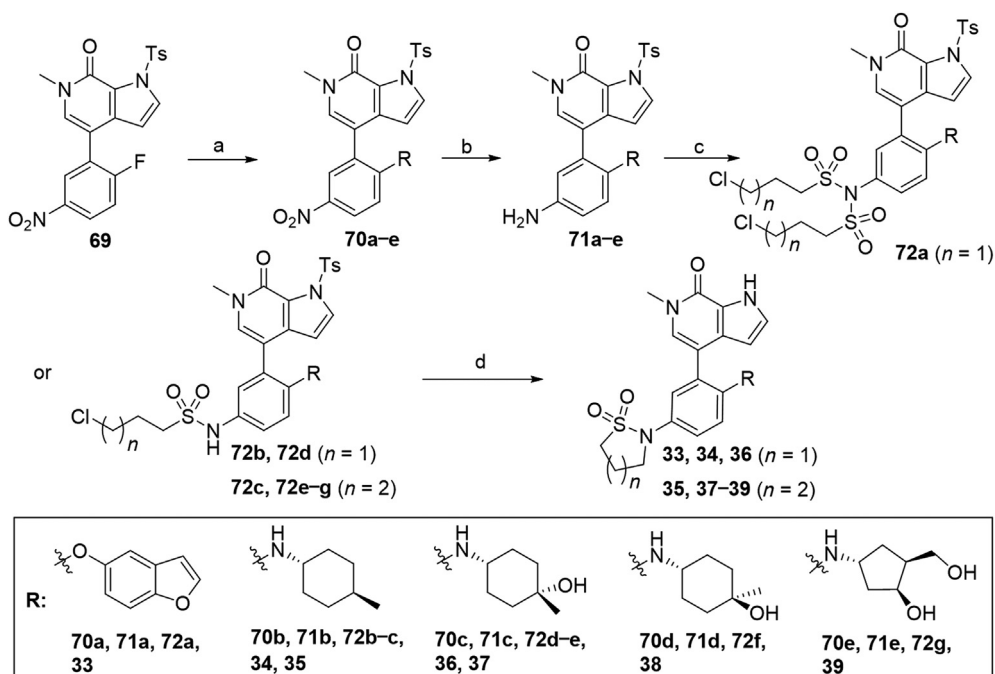
Scheme 7 Synthesis of compounds **33–39**. Reagents and conditions: (a) RH, DIPEA, DMSO, 80 °C, 6 h, 33%–51%; or (for **70a**) RH, K₂CO₃, DMF, r.t., 30 min, 98%; or (for **70b**): i) RH, DMSO, 80 °C, 6 h; ii) TsCl, NaH, DMF, 0 °C, 1 h, 72% over two steps. (b) Pd/C, H₂, 45 °C, CHCl₃/MeOH (1:1), 8 h; or (for **71a**) Fe, NH₄Cl, EtOH/H₂O (5:2), 70 °C, 1 h. (c) 3-Chloropropane-1-sulfonyl chloride or 4-chlorobutane-1-sulfonyl chloride, Et₃N, DCM, r.t., 1 h, 77%–88%; or (for **72g**): i) TMSCl, Et₃N, DMF, 0 °C, 0.5 h; ii) 4-chlorobutane-1-sulfonyl chloride, Et₃N, DCM, r.t., 1 h; (d) NaOH, 1,4-dioxane, 90 °C, 0.5 h, 85%–93%.
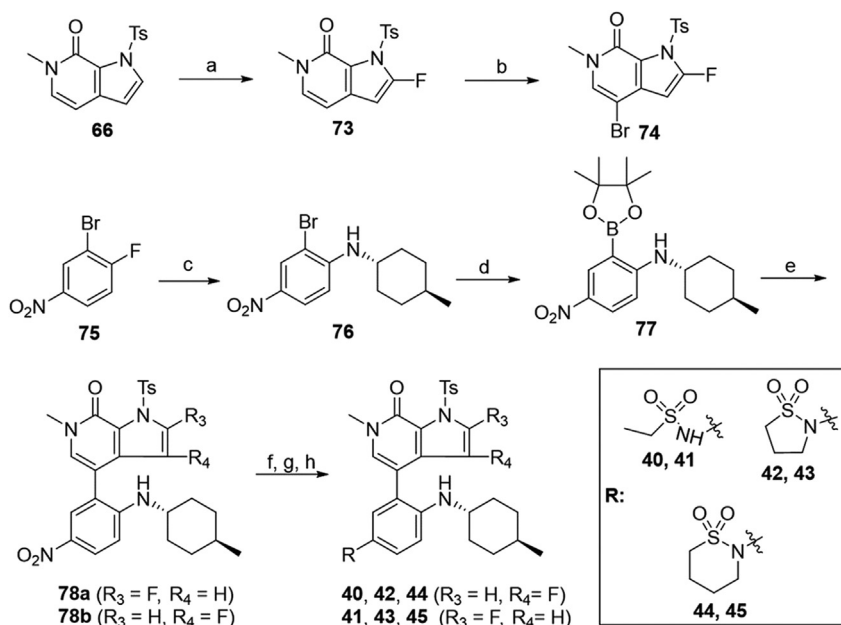
Scheme 8 Synthesis of compounds **40**−**45**. Reagents and conditions: (a) *n*-BuLi, NFSI, dry THF, N_2, −20 °C, 2.5 h, 45%; (b) NBS, TsOH·H_2O, THF, r.t., 1 h; (c) *trans*-4-methylcyclohexyl amine, DMSO, 100 °C, 2 h; (d) bis(pinacolato)diboron, Pd(dppf)Cl_2, AcOK, 1,4-dioxane, N_2, 100, 5 h, 80% over two steps; (e) **63** or **73**, Pd_2(dba)$_3$, meCgPPh, K_3PO_4, dioxane/H_2O (4:1), 80 °C, 5 h, 57%−68%; (f) Pd/C, H_2, 45 °C, CHCl$_3$/MeOH (1:1), 8 h; (g) ethanesulfonyl chloride or 3-chloropropane-1-sulfonyl chloride or 4-chlorobutane-1-sulfonyl chloride, Et$_3$N, DCM, r.t., 1 h, 63%−82%; (h) NaOH, 1,4-dioxane, 90 °C, 0.5 h, 65%−85%.

2.2. Screening of clinical BRD4 inhibitors against HH signaling pathway

To gain insights on the activity relationship between BRD4 and GLI, we selected seven clinically studied BRD4 inhibitors and tested their inhibitory activity in the HH signaling pathway in our dual luciferase reporter assays using light II cells. These cells are NIH-3T3 cells stably transfected with a GLI-responsive firefly luciferase reporter and renilla-luciferase expression vector[21,43]. As shown in Table 1, the seven clinically studied BRD4 inhibitors were found to show high but quite different potency against the HH signaling pathway with IC_{50} values ranging between 0.15 and 40.6 nmol/L. Among them, the phase II BRD4 inhibitor **1** (BMS-986158) is the most potent, whereas INCB-057643 is the least potent HH pathway inhibitor, with IC_{50} values of 0.15 and 40.6 nmol/L, respectively. The overall trend of activity is in agreement with the BRD4 activity where the phase II compound **1** remains the most potent BRD4 inhibitor, and compound **4**[44] (AZD5153) is much less potent, with IC_{50} values of 0.16 and 18.2 nmol/L, respectively. This result indicates that development of high potency GLI-targeting HH pathway inhibitors might be realized by optimization of BRD4 activity through structural modification, since direct structural information on the transcriptional factor GLI is limited. Considering the potential toxicity liability and pharmacokinetic (PK) disadvantage of the tricyclic compounds (*e.g.*, **1** and **3**, Table 1)[35,45], we decided to choose compound **2** (ABBV-075, Table 1) as our lead HH inhibitor for structural optimization. This compound shows high inhibitory activity (0.41 nmol/L) against HH pathway, but is nearly 10-fold less potent against BRD4 (3.4 nmol/L). Our objective is to identify a high potency and well tolerated HH pathway inhibitor for treatment of MB, especially those resistant to current SMO-targeting HH inhibitors.

2.3. Structure-based drug design

4-Aryl-1,6-dihydro-7*H*-pyrrolo[2,3-*c*]pyridin-7-one **2** (ABBV-075, Fig. 2), developed by AbbVie, is a highly potent non-selective BRD4 inhibitor undergoing phase I clinical trials for the treatment of patients with acute myeloid leukemia, multiple myeloma and advanced solid tumors (NCT02391480)[46]. According to the reported co-crystal structure[34] of its close analogue with BRD4 (BD2), the pyrrolopyridone core is located in the KAc binding pocket and provides critical interactions with Asn433 residue. The *meta*-difluorophenoxyl motif fills the WPF hydrophobic shelf (a hydrophobic region constructed by residues W81, P82 and F83), and the ethyl sulfonamide chain occupies the ZA channel of the BRD4 (BD2) protein. In addition, the pyrrole fragment and the ethyl sulfonamide chain are both exposed to the solvent interaction region, which may tolerate various substituents. Inspired by this analysis and in view of the lack of targetable binding domains of the transcriptional factors GLI[20], we have designed several series of analogues by modifying these interaction sites through three approaches, including: (1) opening the pyrropyridinone bicyclic core to afford flexible 3-aminopyridiones; (2) cyclizing the ethanesulfonamide motif; (3) replacing the hydrophobic difluorophenyl with a water soluble moiety (Fig. 1).

2.4. Structure−activity relationship (SAR) study

To investigate how the structural alterations impact activities of GLI, we first cleaved the bicyclic pyrrolopyridone core of compound **2** in 3-aminopyridinones **5**−**11**. As shown in Table 2, all these compounds are much less potent than compound **2**. Carbamate **5** has an IC_{50} value of 27.6 nmol/L against BRD4, which is 8-fold less potent than that of **2**. Both carbamate **6** with a longer chain and the reverse amide **7** show more reduction of potency. 3-

Table 1   Inhibition of clinical BRD4 inhibitors against BRD4 BD1 and the HH pathway[a].

Compd.	Clinical stage	Structure	IC$_{50}$ (nmol/L)	
			BRD4 (BD1)	GLI-luc
BMS-986158 (**1**)	I/II		<0.16	0.15 ± 0.05
ABBV-075 (**2**)	I		3.4 ± 0.2	0.41 ± 0.34
PLX51107	I		0.49 ± 0.14	5.5 ± 1.3
OTX-015	II		7.7 ± 0.21	0.64 ± 0.02
JQ1 (**3**)	Discovery		9.8 ± 2.2	2.6 ± 1.7
INCB-057643	I/II		11.6 ± 1.8	40.6 ± 4.9
AZD5153 (**4**)	I		18.2 ± 2.7	32.1 ± 7.71

[a]IC$_{50}$ values are shown as the mean ± SD (nmol/L) from three separate experiments.
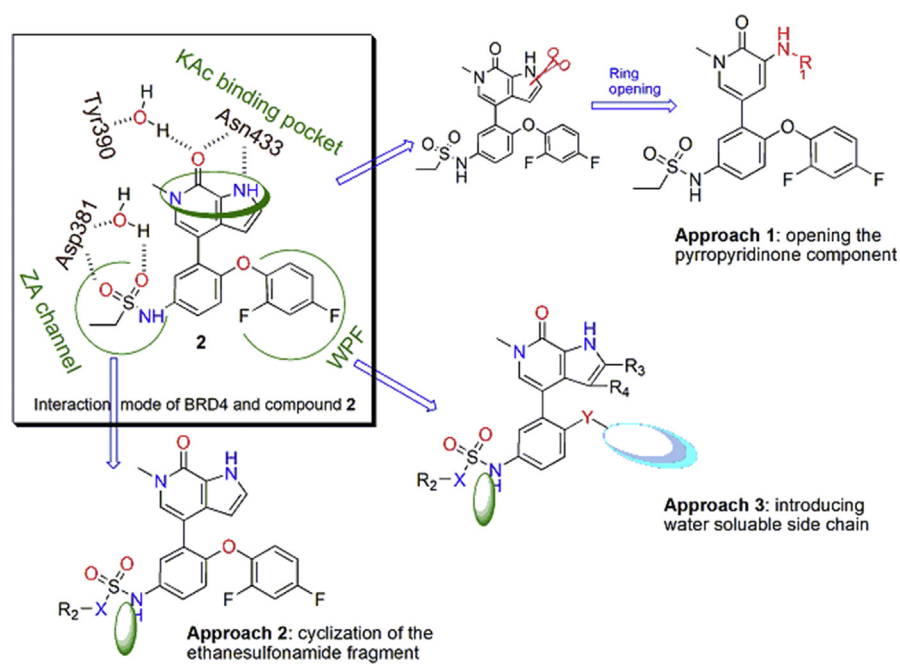
Figure 2   Structural analysis and design of new HH pathway inhibitors.

Ethanesulfonamido pyridinone **8** and 3-((1*H*-imidazol-2-yl) amino) pyridinone **9** display modest potency against BRD4 with IC_{50} value of 42.8 and 47.6 nmol/L, respectively. *N*-Heterocycle-substituted 3-aminopyridinones **10** and **11** show much reduced potency with IC_{50} values greater than 100 nmol/L. These results indicate that although the substituted 3-amino analogues may maintain the H-bonding with Asn433 residue in the KAc binding pocket of BRD4 (BD1), the electronic or steric property potentially affects the interaction with BRD4 as well. Disappointingly, all the compounds show markedly reduced potency against the HH pathway with IC_{50} values all greater than 100 nmol/L in the GLI-luciferase assay.

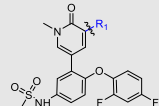Next, considering that there is a large space in the ZA channel interaction region in the binding mode of **2** with BRD4 (PDB code: 5uvx)[34], we evaluated compounds derived from cyclization of the ethanesulfonamide. As shown in Table 3, the five- and six-membered cyclic sulfonamides **12** and **13** display much higher potency against BRD4 with IC_{50} values of 0.25 and 0.60 nmol/L, respectively. However, their potency against the HH pathway is significantly reduced with IC_{50} values of 3.29 and 20.5 nmol/L, respectively. In order to increase aqueous solubility (Table 7), we incorporated an additional N-atom moiety with various substituents leading to compounds **14−23**. Most of these N-substituted cyclic aminosulfonamides except **16** and **22** were found much more potent than **2**, by showing low- or sub-nanomolar potency against BRD4. However, all compounds are significantly less potent than **2** against the HH pathway with IC_{50} values between 17.7 and 100 nmol/L. Compound **22** bearing a substituted pyrrolidinylethyl moiety has the least potency in both assays. The five-membered analogues are slightly more potent than the six-membered congeners, especially against BRD4.

These results indicate that the ZA channel of BRD4 BD1 can tolerate various substitutions, whereas larger substituents are not beneficial for interaction with the HH pathway.

As shown in Table 4, our next effort is to incorporate fluoro or other electron-withdrawing substituent on the C2- or C3-position of the pyrrolopyridone skeleton to the cyclic analogues of ethane-sulfonamide motif. Compounds **24** and **25**, both with a fluoro-substituent at the C3-position of the pyrrole component, display high potency against BRD4 and the HH pathway with IC_{50} values ranging between 0.48 and 1.5 nmol/L. However, compounds **26** and **27** bearing a carboxylic group at the C2-position of the pyrrole component show >4-fold decrease of potency against BRD4, together with markedly reduced potency (>100 nmol/L) against the HH pathway. Pleasantly, high potency was observed for compounds **28−32** containing an amide moiety at the C2-position of the pyrrole component. The unsubstituted carboxamides **28** and **29** show an identical IC_{50} value of 0.09 nmol/L against BRD4, whereas their potency against the HH pathway is slightly lower by showing IC_{50} values of 1.5 and 2.46 nmol/L, respectively. *N*-Ethyl substituted amide analogues **30** and **31** also display high potency, especially compound **30** having IC_{50} values of 0.6 and 0.05 nmol/L, respectively against BRD4 and the HH pathway, which are much more

Table 2 Inhibition of compounds against BRD4 (BD1) and the HH pathway[a].
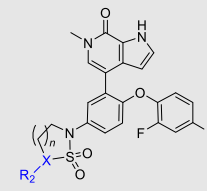
Compd.	R_1	IC_{50} (nmol/L)	
		BRD4 (BD1)	GLI-luc reporter
5		27.6 ± 5.7	157 ± 1.3
6		>100	>100
7		>100	>100
8		42.8 ± 9.6	>100
9		47.6 ± 2.9	>100
10		>100	>100
11		>100	>100
ABBV-075 (**2**)	−	3.4 ± 0.2	0.41 ± 0.34

[a]IC_{50} values are shown as the mean ± SD (nmol/L) from three separate experiments. −Not applicable.

Table 3 Inhibition of compounds against BRD4 (BD1) and the HH pathway[a].

Compd.	X	*n*	R_2	IC_{50} (nmol/L)	
				BRD4 (BD1)	GLI-luc reporter
12	C	1	CH_2OH	0.25 ± 0.05	3.29 ± 0.14
13	C	2	CH_2OH	0.60 ± 0.07	20.5 ± 7.74
14	N	1		0.20 ± 0.03	26.1 ± 5.17
15	N	1		1.19 ± 0.10	71.9 ± 5.43
16	N	2		9.39 ± 0.80	28.9 ± 11.9
17	N	2		0.65 ± 0.36	33.9 ± 11.1
18	N	2		1.52 ± 0.72	56.1 ± 8.25
19	N	2		1.47 ± 0.03	17.7 ± 11.0
20	N	2		1.01 ± 0.34	42.8 ± 30.7
21	N	2		0.99 ± 0.19	39.4 ± 4.76
22	N	2		71.9 ± 5.43	>100
23	N	2		0.58 ± 0.10	45.8 ± 19.2
2	−	−	−	3.4 ± 0.2	0.41 ± 0.34

[a]IC_{50} values are shown as the mean ± SD (nmol/L) from three separate experiments. −Not applicable.

Table 4 Inhibition of compounds against BRD4 (BD1) and the HH pathway[a].
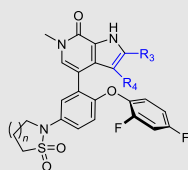
Compd.	n	R_3	R_4	IC$_{50}$ (nmol/L)	
				BRD4 (BD1)	GLI-luc reporter
24	1	H	F	0.50 ± 0.06	0.93 ± 0.16
25	2	H	F	1.51 ± 0.43	0.48 ± 0.08
26	1	COOH	H	21.0 ± 11.0	>100
27	2	COOH	H	14.3 ± 4.52	>100
28	1	CONH$_2$	H	0.09 ± 0.04	1.5 ± 0.39
29	2	CONH$_2$	H	0.09 ± 0.08	2.46 ± 0.3
30	1	CONHCH$_2$CH$_3$	H	0.60 ± 0.41	0.05 ± 0.01
31	2	CONHCH$_2$CH$_3$	H	0.13 ± 0.005	0.81 ± 0.24
32	1	(structure)	H	0.75 ± 0.07	>100
2	–	–	–	3.4 ± 0.2	0.41 ± 0.34

[a]IC$_{50}$ values are shown as the mean ± SD (nmol/L) from three separate experiments. −Not applicable.

Table 5 Inhibition of compounds against BRD4 (BD1) and the HH pathway[a].
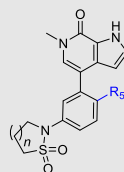
Compd.	n	R_5	IC$_{50}$ (nmol/L)	
			BRD4 (BD1)	GLI-luc reporter
33	1	(benzofuran)	2.85 ± 0.50	1.03 ± 0.28
34	1	(4-methylcyclohexyl amino)	0.52 ± 0.03	0.12 ± 0.1
35	2	(4-methylcyclohexyl amino)	0.99 ± 0.01	0.33 ± 0.13
36	1	(structure)	1.24 ± 0.09	1.58 ± 0.66
37	2	(structure)	2.60 ± 056	1.47 ± 0.66
38	2	(structure)	3.22 ± 0.11	1.34 ± 0.48
39	2	(structure)	3.42 ± 0.25	>100
2	–	–	3.4 ± 0.2	0.41 ± 0.34

[a]IC$_{50}$ values are shown as the mean ± SD (nmol/L) from three separate experiments. −Not applicable.

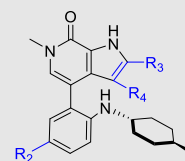**Table 6** Inhibition of compounds against BRD4 (BD1) and the HH pathway[a].

Compd.	R_2	R_3	R_4	IC$_{50}$ (nmol/L)	
				BRD4 (BD1)	GLI-luc reporter
40	(structure)	H	F	14.25 ± 2.76	2.06 ± 1.16
41	(structure)	F	H	17.57 ± 0.55	5.88 ± 2.72
42	(structure)	H	F	9.51 ± 1.13	0.33 ± 0.056
43	(structure)	F	H	14.28 ± 1.27	0.062 ± 0.039
44	(structure)	H	F	19.10 ± 3.55	0.58 ± 0.35
45	(structure)	F	H	20.52 ± 1.18	1.75 ± 0.63
2	–	–	–	3.4 ± 0.2	0.41 ± 0.34

[a]IC$_{50}$ values are shown as the mean ± SD (nmol/L) from three separate experiments. −Not applicable.

potent than compound **2**. However, amide **32** with a longer N-substituent shows much reduced potency (>100 nmol/L) against the HH pathway, despite of the high potency for BRD4.

Meanwhile, structural modification of the WPF interaction region of BRD4 (BD1) was conducted based on the ethanesulfonamide motif cyclized analogues. As shown in Table 5, compound **33** containing a benzofuran moiety to replace the original 2,4-difluorophenyl group maintains good potency against BRD4 (2.85 nmol/L), whereas the potency for the HH pathway was reduced (1.03 nmol/L). Compounds **34−39** all contain a water soluble substituent to replace the original phenylether motif. Compared to **2**, these compounds generally retain good potency against BRD4, but the activity against the HH pathway is distinctly different. Notably, compounds **34** and **35** both bearing a 4-methylcyclohexyl amino substituent show extremely high potency in both assays, although the five-membered analogue **35** is slightly less potent than the six-membered analogue **34**. Indeed, compound **34** is the most potent analogue among this series and shows IC$_{50}$ values of 0.52 and 0.12 nmol/L, respectively against BRD4 and the HH pathway, and is 6.5- and 3.4-fold more potent than compound **2**. Incorporation of an additional *C*4-hydroxyl group on the cyclohexyl (compounds **36** and **37**) or reversing the chirality of the resulting quaternary carbon (compound **38**) led to no improvement with IC$_{50}$ values ranging between 1.2 and 3.4 nmol/L for both BRD4 and the HH pathway. In addition, compound **39** bearing a (3-hydroxy-4-hydroxymethyl) cyclopentylamino substituent lost the activity against the HH pathway significantly, despite remaining high potency for BRD4.

Based on the optimization results, we collected all the advantageous elements and incorporated them into a small series of multisubstituted pyrropyridinone analogues bearing a 4-methylcyclohexan-1-amino motif in the WPF binding site. As

Table 7   hERG inhibition and predicted physico-chemical parameters of representative compounds[a].

Compd.	GLI-luc reporter IC$_{50}$ (nmol/L)	BRD4 IC$_{50}$ (nmol/L)	hERG IC$_{50}$ (μmol/L)	tPSA[b] (Å)	LogS[b] (μg/mL)	LogP$_{app}$[b] (cm/s)	VD[b] (L/kg)
43	0.062 ± 0.039	14.28 ± 1.27	—	87.2	17.88	−5.228	−0.24
30	0.05 ± 0.01	0.60 ± 0.41	6.4	113	21.35	−5.135	−0.795
34	0.12 ± 0.1	0.52 ± 0.03	>40	87.2	17.60	−5.194	−0.034
35	0.33 ± 0.13	0.99 ± 0.01	>40	87.2	17.94	−5.235	−0.078
25	0.48 ± 0.08	1.51 ± 0.43	27.3	84.4	9.14	−4.79	−0.551
24	0.93 ± 0.16	0.50 ± 0.06	>40	84.4	18.14	−4.773	−0.518
31	0.81 ± 0.24	0.13 ± 0.005	11.7	113	30.16	−5.164	−0.799
33	1.03 ± 0.28	2.85 ± 0.50	—	97.5	9.35	−5.312	−0.345
28	1.5 ± 0.39	0.09 ± 0.04	>40	127	51.80	−5.189	−0.754
2	0.41 ± 0.34	3.4 ± 0.2	35.5	93.2	19.60	−5.01	−0.547

[a]IC$_{50}$ values are shown as the mean ± SD (nmol/L) from three separate experiments.
[b]Calculated through ADMET lab software *via* http://admet.scbdd.com; tPSA, topological polar surface area; logS, solubility; P$_{app}$, Caco-2 permeability; VD, volume distribution. —Not applicable.

shown in Table 6, compared to the high potency of compound **34**, all these compounds show reduced potency against BRD4 with IC$_{50}$ values ranging between 9.51 and 20.54 nmol/L. The potency for the HH pathway is also decreased but distinctly different. Similarly modest potency was observed for compounds **40** and **41** in both assays indicating that there is no significant difference for the fluoro substituent on either the C2- or C3-position of the pyrrole component. Dramatically, compounds **42**−**45** with the ethanesulfonamido component cyclized to five- or six-membered sulfonamides show higher potency for the HH pathway, though their potency against BRD4 is modest, suggesting that the interaction mode for the HH signaling is different from that for BRD4. Among these, compound **43** is the most potent HH pathway inhibitor with IC$_{50}$ values of 0.062 nmol/L, and shows 230-fold selectivity against BRD4.

2.5.   hERG inhibition and predicted physico-chemical properties of potent compounds

From the SAR, we concluded that the inhibitory activity against BRD4 does not completely parallel with the potency of the HH pathway. Overall, BRD4 is well tolerant to various substitutions, whereas the activity for the HH pathway is much different and highly dependent on different substitution patterns. As listed in Tables 7 and 9 new compounds turn out as the high potency HH inhibitors with IC$_{50}$ values less than 1.5 nmol/L. The most potent HH inhibitor **43** has an IC$_{50}$ value of 0.062 nmol/L and is 230-fold more potent than against BRD4 (14.28 nmol/L), whereas compound **28**, though highly potent against BRD4 (0.09 nmol/L), is 16-fold less potent for the HH pathway (1.5 nmol/L).

To investigate the safety and druglikeness of these new HH inhibitors, we tested their inhibition on hERG channel and predicted their physico-chemical properties. As shown in Table 7, most compounds except **30** and **31** show negligible inhibition on the hERG with IC$_{50}$ values greater than 20 μmol/L, indicating their low liability of cardiac toxicity. Compounds **30** and **31** have IC$_{50}$ values of 6.4 and 11.7 μmol/L, indicating their slightly safety concerns on hERG, likely due to their more basic nature since both compounds contain a carboxamide substituent on the pyrrolopyridone component. Meanwhile, most compounds have similar predicated physico-chemical properties, including acceptable tPSA (<140 Å), modest aqueous solubility (logS), and low Caco-2 permeability (Table 7).

Table 8   PK parameters of potent compounds after *p.o.* (3 mg/kg) and i.v. (1 mg/kg) administration.

Compd.	Route	$t_{1/2}$ (h)	T_{max} (h)	C_{max} (ng/mL)	AUC$_{last}$ (h·ng/mL)	AUC$_{INF\_obs}$ (h·ng/mL)	CL$_{obs}$ (mL/min/kg)	MRT$_{INF\_obs}$ (h)	Vss$_{obs}$ (mL/kg)	F
24	*p.o.*	0.95	0.50	474	473	473	—	1.26	—	30.9
	i.v.	0.56	—	—	509	509	33.2	0.76	1513	—
25	*p.o.*	0.96	0.25	503	406	406	—	0.95	—	22.0
	i.v.	0.54	—	—	614	614	27.2	0.77	1258	—
30	*p.o.*	1.35	0.25	15.2	9.91	9.91	—	0.89	—	1.2
	i.v.	0.68	—	—	278	278	61.5	0.794	2891	—
31	*p.o.*	1.55	0.33	15.5	18.3	22.1	—	2.38	—	2.9
	i.v.	0.69	—	—	213	217	77.6	0.57	3512	—
34	*p.o.*	2.06	1.00	29.1	97.3	107	—	3.49	—	12.7
	i.v.	1.09	—	—	255	261	76.4	1.66	8781	—
35	*p.o.*	1.00	0.5	110	190	190	—	1.54	—	21.0
	i.v.	1.06	—	—	300	300	59.2	1.20	4211	—
43	*p.o.*	2.02	0.42	346	861	924	—	3.18	—	4.71
	i.v.	1.05	—	—	6099	6135	2.78	1.46	239	—
2	*p.o.*	3.34	2.75	401	2030	2052	—	5.45	—	57.0
	i.v.	2.74	—	—	1186	1195	17.6	3.11	2772	—

[a]Values are the average of three runs. Vehicle: *p.o.*, DMSO/0.5% HPMC (5/95, *v/v*); i.v., EtOH/PEG300/NaCl (10/40/50, *v/v/v*). CL, clearance; Vss, volume of distribution; $t_{1/2}$, half-life; AUC, area under the plasma concentration time curve; F, oral bioavailability. —Not applicable.

Table 9 Antiproliferative inhibition of various cancer cells.

GI$_{50}$[a] (µmol/L)	H3132	N87	HT1080	Colo680N	HSC-2	KYSE450	TOV-21G	CAL27	SKM-1	H1975	DOHH-2	MOLM-14	MV4-11	TMD8	REC-1	CHL
25	0.14	0.13	1.0	2.3	0.77	1.6	0.023	0.11	0.019	0.034	0.0066	0.0081	0.0035	0.0093	0.015	>10
35	0.33	0.46	0.88	4.0	0.32	1.4	0.008	0.12	0.0063	0.0054	0.0021	0.002	0.0013	0.0022	0.0022	1.1

[a]Antiproliferative effects were initially tested in 10 µmol/L, and then diluted in eight diluted concentrations. GI$_{50}$ values were obtained from two separate experiments.

2.6. Pharmacokinetic parameters of potent compounds

To select optimal compound for further *in vitro* and *in vivo* antitumor study, the 7 highly potent HH inhibitors with IC$_{50}$ values less than 1.0 nmol/L were selected for further evaluation for their pharmacokinetic (PK) parameters in Sprague−Dawley rats dosed intravenously (i.v., 1 mg/kg) and orally (p.o., 3 mg/kg). As shown in Table 8, these compounds generally have short half-life ($t_{1/2}$)
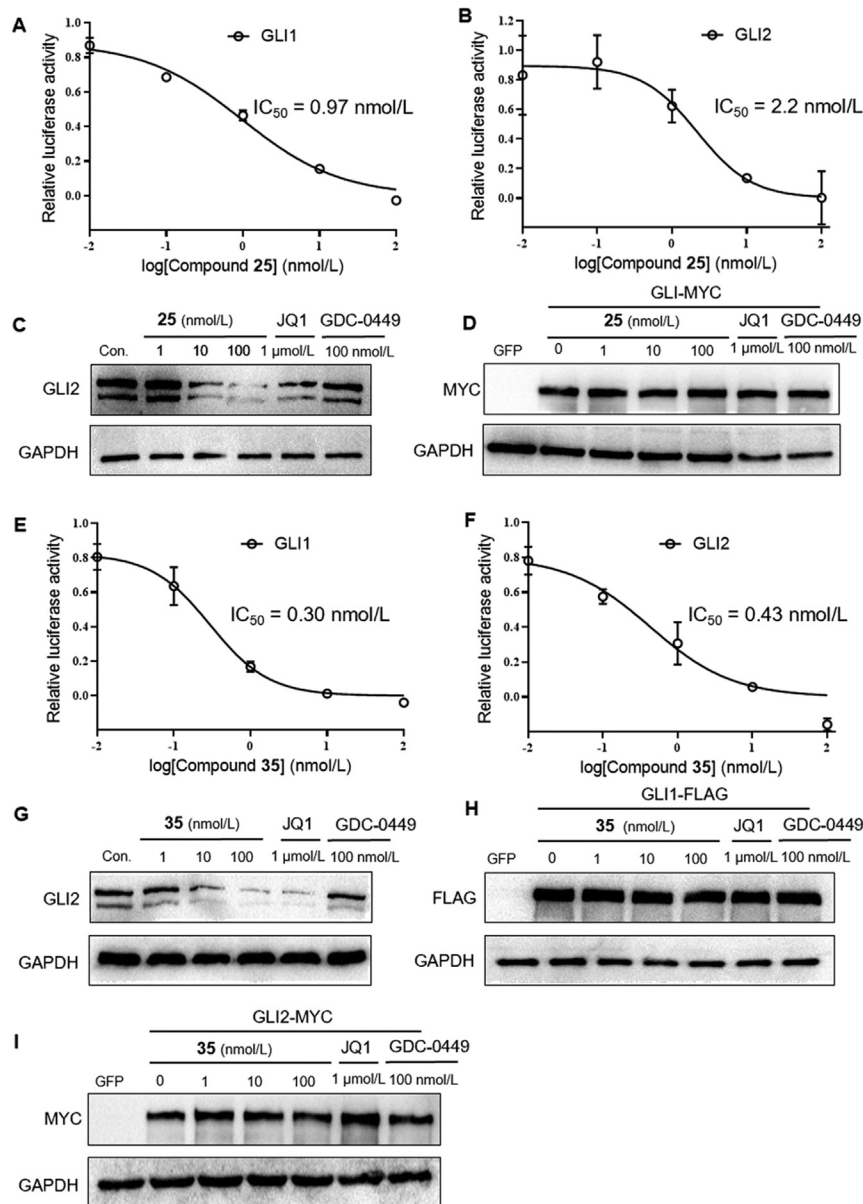

Figure 3 Compounds **25** and **35** inhibit HH activity at the level of GLI1/2. (A), (B) and (E), (F): GLI-luciferase activity in light2 cells treated with **25** or **35** after transfection with GLI1 or GLI2 construct; (C) and (G): Western blots evaluating endogenous GLI2 expression in light2 cells after treatment with **25**, **35**, JQ1 (1 µmol/L), and GDC-0449 (100 nmol/L); (D) and (H): GLI2-MYC protein expressions in light2 cells transfected with GLI2-MYC; (I): Western blots analysis of exogenous GLI1-FLAG.

and modest plasma exposure (AUC). Compounds **24**, **25** and **35** have relatively acceptable oral bioavailability (20%−30%) and modest clearance. Unfortunately, the most potent HH inhibitors **43** (0.062 nmol/L) and **30** (0.05 nmol/L) display poor PK parameters, especially with scarce oral bioavailability. Therefore, after consideration of the HH inhibitory potency and PK profile, we chose compounds **25** and **35** for further investigation.

2.7. Antiproliferative effects of compounds 25 and 35 against various cancer cells

Since the HH signaling pathway is a major regulator governing cell proliferation and differentiation, the selected HH inhibitors **25** and **35** were tested for their antiproliferative effects against a wide spectrum of cancer cell lines, including nine solid and six hematologic tumor cell lines, together with the CHL normal cell line. As shown in Table 9, no or low inhibition on the normal CHL cell lines

was observed, especially for compound **25** with an GI_{50} value greater than 10 μmol/L, indicating the high selectivity against cancer cells. Notably, compared to the solid tumor cells, both compounds show markedly higher potency in the hematologic tumor cell lines, especially for SKM-1, DOHH-2, MOLM-14, MV4-11, MOLM-13 and TMD8 cell lines with GI_{50} value less than 10 nmol/L.

2.8. Inhibition of HH signaling pathway at the level of GLI

To investigate the exact mechanism of compounds **25** and **35** within the HH signaling pathway[28], we investigated the suppressing effects of both compounds in the HH pathway by overexpressing GLI1 or GLI2. As shown in Fig. 3, compound **25** significantly inhibited GLI-luciferase activity provoked by forced expression of GLI1 or GLI2, with IC_{50} values of 0.97 and 2.2 nmol/L, respectively (Fig. 3A and B). Meanwhile, compound **25** dramatically reduced the abundance of endogenous GLI2 proteins in light2 cells at concentration of both 10
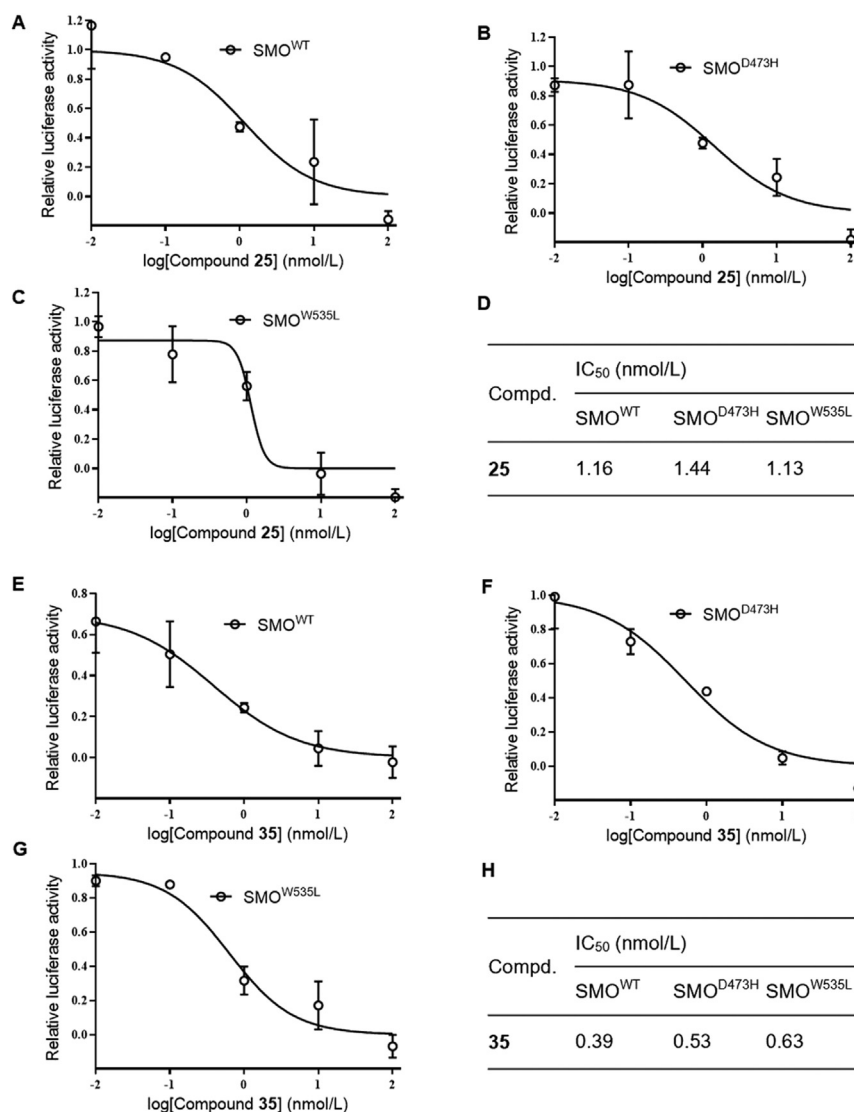

Figure 4   Compounds **25** and **35** possess *in vitro* ability of circumventing the resistance to SMO inhibitors caused by SMO mutations. GLI-luciferase analysis of the inhibitory effects of compounds in light2 cells followed by transfection with SMO^{WT} (A) and (E), $SMOD^{473H}$ (B) and (F), or SMO^{W535L} (C) and (G), respectively. (D) and (H) IC_{50} values of compounds in light2 cells with forced expression of SMO^{WT}, SMO^{D473H} and SMO^{W535L}.
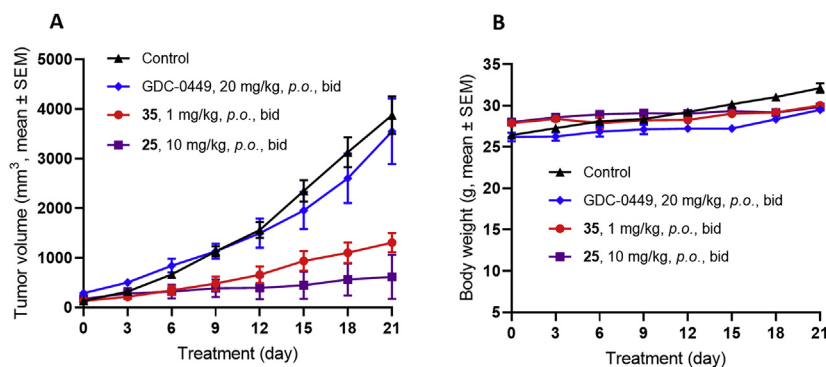
Figure 5 Antitumor activity of compounds **25** and **35** in SMOA1 MB allograft model. Nude mice with subcutaneously transplanted SMOA1 MB allografts were treated with vehicle control (0.5% CMC-Na, *p.o.*, bid), compounds **25** and **35** (*p.o.*, bid) or GDC-0449 (*p.o.*, bid). (A) Tumor volume and (B) body-weight change over time in treated SMOA1 MB allograft. Data represent group means ± SEM (control, $n = 4$; GDC-0449, $n = 4$; **35**, $n = 4$; **25**, $n = 3$).

and 100 nmol/L, and the effect on GLI2 proteins of compound **25** (100 nmol/L) is superior to JQ1 (1 μmol/L), whereas the SMO inhibitor GDC-0449 (vismodegib) has no effect on the expression of endogenous GLI2 (Fig. 3C). In addition, compound **25** failed to inhibit the expression of exogenous GLI2-MYC (Fig. 3D).

Similarly, compound **35** also inhibited GLI-luciferase activity provoked by forced expression of GLI1 or GLI2, with IC_{50} values of 0.30 and 0.43 nmol/L, respectively (Fig. 3E and F). Meanwhile, compound **35** down-regulated endogenous GLI2 proteins in light2 cells (Fig. 3G), whereas no effect was observed on the expression of exogenous GLI1-FLAG and GLI2-MYC (Fig. 3H and I).

Given the fact that significant suppression on the HH activation provoked by forced expression of GLI1 or GLI2 was observed by compounds **25** and **35**, but not by SMO inhibitor, as well as the robust inhibition of **25** and **35** on the activity of BRD proteins, we conclude that compounds **25** and **35** epigenetically inhibit HH signaling pathway at the level of GLI, not at the upstream targets of the HH signaling pathway, *e.g.*, SMO.

2.9. Compounds 25 and 35 can circumvent drug resistance caused by SMO mutations

Having characterized that compounds **25** and **35** function as HH inhibitors by acting at the level of GLI, we continued to evaluate its *in vitro* ability of combating the resistance to SMO inhibitors

caused by SMO mutation[47]. As expected, both compounds markedly blocked GLI-luciferase activity in light2 cells induced by ectopic expression of wild type SMO (SMO^{WT}, Fig. 4A and E), as well as SMO^{D473H} (Fig. 4B and F) and SMO^{W535L} (Fig. 4C and G), two most predominant mutants[47] of SMO responsible for the resistance to SMO inhibitors, with respective IC_{50} values of 1.16, 1.44 and 1.13 nmol/L for **25**, and 0.39, 0.53 and 0.63 nmol/L for **35** (Fig. 4D and H). These findings indicate that compounds **25** and **35** are promising HH inhibitors with capacity of overcoming drug resistance caused by SMO mutations.

2.10. In vivo antitumor effects in SMOA1 MB allograft model

To translate the *in vitro* ability of the GLI inhibitors **25** and **35** in combating the resistance caused by SMO inhibition into *in vivo* antitumor efficacy, we established spontaneous SMOA1 MB model, of which tumors contain mutation at the amino acid residue 539 of SMO (SMO^{W539L}), and are resistant to current SMO inhibitor vismodegib (GDC-0449) in ND2:SMOA1 mice[48]. As shown in Fig. 5A, treatment with compound **25** at 10 mg/kg by oral administration (*p.o.*, bid) realized 88.2% tumor growth inhibition (TGI), whereas the SMO inhibitor GDC-0449 failed to affect the tumor growth at 20 mg/kg (*p.o.*, bid), a dosage resulting in complete tumor growth inhibition in SMO wild MB mice[49].
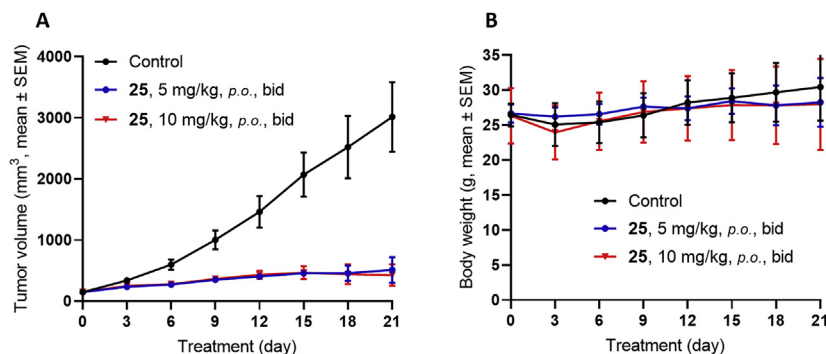

Figure 6 Antitumor activity of compound **25** in SMOA1 MB allograft model. Nude mice with subcutaneously transplanted SMOA1 MB allografts were treated with vehicle control (0.5% CMC-Na, *p.o.*, bid), or compound **25** (*p.o.*, bid). (A) Tumor volume and (B) body-weight change over time in treated SMOA1 MB allograft. Data represent group means ± SEM (control, $n = 4$; **25**, 5 mg/kg, $n = 4$; **25**, 10 mg/kg, $n = 5$).

However, despite its higher potency of **35** *in vitro* than compound **25**, treatment of this compound at the same dosage was not tolerated leading to significant casualty (data are not shown). However, a lower dose of **35** at 1 mg/kg was well tolerant with TGI of 68.7%. No obvious body weight loss was observed in both the 10 mg/kg group of **25** and the 1 mg/kg group of **35** during treatment (Fig. 5B). These results suggest that both compounds **25** and **35** are capable of combating SMO inhibitor-resistant MB tumors.

Since compound **25** functioned as an efficacious and more tolerant GLI inhibitor than compound **35** to overcome the resistant MB tumors caused by SMO^{W539L} mutation, we continued to evaluate this compound at lower dosage. As shown in Fig. 6A, compound **25**, even at a lower dosage of 5 mg/kg (*p.o.*, bid) still shows 83.3% tumor growth inhibition, similar to the effect of 10 mg/kg dose (TGI = 87.6%). Meanwhile, the new HH inhibitor **25** was well tolerant in both doses without significant overall toxicity (Fig. 6B).

3. Conclusions

In summary, by repurposing a series of the clinically investigational BRD4 inhibitors as the HH signaling pathway inhibitors, the AbbVie's phase I clinical pan-BET inhibitor **2** (ABBV-075) was selected for a systemic medicinal chemistry optimization. The established SAR indicates that the inhibitory activity against BRD4 does not parallel with the potency for the HH pathway. Notably, BRD4 is well tolerant to various substitution patterns, whereas the activity for the HH pathway is much different and highly dependent on the steric and electrostatic natures of the substituents. A number of compounds were identified showing IC_{50} values less than 1.0 nmol/L against the HH signaling pathway, and further investigation of their inhibition on hERG and PK parameters elected compounds **25** and **35** as the high potency HH inhibitors. Similar to compound **2**, these new compounds are non-selective BET inhibitors (Supporting Information Fig. S2 and Table S2) that might be more effective to modulate GLI activity. Further mechanism profiling showed that the two new compounds suppressed HH signaling by interaction with the transcriptional factor GLI, and are equally potent against both the two clinically identified resistant SMO mutants (SMO^{D473H} and SMO^{W535L}) and SMO wild type, with IC_{50} values around 1 nmol/L or less. Although the PK parameters are not optimal, both compounds showed significant antitumor efficacy *in vivo* in the resistant MB allograft mice. Compared to the dose-limited toxicity of compound **35**, compound **25** was more tolerant and significantly suppressed tumor growth at both 5 mg/kg (TGI = 83.3%) and 10 mg/kg (TGI = 87.6%) doses. Therefore, the new GLI inhibitor **25** represents not only a high potent HH inhibitor both *in vitro* and *in vivo*, but also a relatively safe and tolerant lead compound capable of suppressing HH-driven MB, that is resistant to current SMO antagonists.

4. Experimental

4.1. Chemistry

All reactions were performed in glassware containing a teflon-coated stir bar. All commercially purchased reagents and solvents were chemical pure and used without futher purification. ^{1}H NMR and ^{13}C NMR spectra were recorded on a Varian Mercury 300,

400 or 500 NMR spectrometer (Bruker Biospin AG, Romanshorn, Switzerland) and referenced to deuterium dimethyl sulfoxide (DMSO-d_6), deuterium chloroform (CDCl$_3$), deuterium methanol (CD$_3$OD) or deuterium dichloromethane (CD$_2$Cl$_2$). Chemical shifts (δ) were reported in ppm downfield from an internal TMS standard. High-resolution mass spectrometry (HRMS) analysis was recorded at anionizing voltage of 70 eV on a Finnigan/MAT95 spectrometer (Agilent, Palo Alto, CA, USA). Flash column chromatography on silica gel (200−300 mesh, Yucheng chemical, Shanghai, China) was used for the routine purification of reaction products. All reactions were monitored by TLC on silica gel plates (50 mm × 15 mm) and spots were visualized under UV light (Changbo, Shanghai, China). Melting points were determined using a SGW X-4 hot stage microscope (INESA, Shanghai, China) and are uncorrected. HPLC analysis was conducted for all bioassayed compounds on an Agilent Technologies 1260 series LC system (ZORBAX-C18 (150 mm × 4.6 mm, Daicel, Shanghai, China), 5 μmol/L, MeOH/H$_2$O or MeCN/H$_2$O, r.t.) with two ultraviolet wavelengths (UV 254 and 214 nm). The purities of these compounds were above 95%.

4.2. Synthetic procedures

Synthesis of target compounds and key intermediates was shown in Supporting Information. Compounds **46**, **51**, **60a**, **66** and **75** were commericially purchased, and compounds **47**[35], **53**[49], **55**[49], **60**[42] and **69**[34] were prepared according to corresponding literature procedures.

4.3. Biological studies

4.3.1. Homogeneous time-resolved fluorescence
The binding of compounds to BRD4 was assessed using an homogeneous time-resolved fluorescence assay. Recombinant BRD4 proteins (Active Motif, Cat#31380 and 31446, Carlsbad, CA, USA), compounds and peptide were diluted to desired working concentrations with EPIgenerous binding buffer (Cisbio, Cat#62DLBDDF, Codolet, France). 4 μL of 5 × BRD4 protein at 165 ng/mL, 4 μL of 5 × biotin labeled acetylated H4K5/K8/K12/K16 at 200 ng/mL and 2 μL of serial diluted test compounds were added to the wells of a 384 ProxiPlate (PerkinElmer, Cat#6008289, Waltham, MA, USA). After 30 min incubation at 37 °C, a 10 μL mixture of IgG antibody labeled with Eu and streptavidin labeled with XL665 were prepared and added to each well for 3 h to reach equilibrium at room temperature. The signal of fluorescence was detected on Envison (PerkinElmer) and analyzed in GraphPad Prism (San Diego, CA, USA).

4.3.2. Dual luciferase reporter assay
Light2 cells (ATCC, Manassas, VA, USA) were treated with compounds as indicated for 36 h. Relative-luciferase assays were performed using dual-luciferase reporter assay kit (Promega, Madison, WI, USA) according to manufacturer's instructions. Relative luciferase values were normalized to TK-renilla value.

4.3.3. Cell growth inhibition assays
SKM-1 cells (JCRB, Osaka, Japan) were seeded into a 96-well plate at a suitable density in a volume of 100 μL medium. After incubation overnight, compounds dissolved in DMSO stock solutions were thawed at room temperature and diluted to the desired concentrations with saline. The compounds were added and cultured for 72 h, the IC_{50} (or GI_{50}) value was measured with

the Cell Counting Kit-8 (CCK-8) assay (Dojindo, Kumamoto, Japan).

4.3.4. GLI protein expression assays

Light2 cells were transfected with MYC-GLI2-FL or FLAG-GLI1 (Addgene, Cambridge, MA, USA) using Lipo2000 (Invitrogen, Carlsbad, CA, USA) as manufacturer's protocol. Cells were treated with indicated compounds 24 h after transfection.

4.3.5. Western blot analysis

Cells were lysed with LDS Sample Buffer (NP0008, Life, Waltham, MA, USA). The protein samples were analyzed with SDS-PAGE gel (Cell Signaling Technology, Boston, MA, USA) and immunoblotted with the following primary antibodies: anti-HA, anti-FLAG, anti-GLI2 (1:1000, Cell Signaling Technology) or GAPDH (1:5000, Santa Cruz Biotechnology, Santa Cruz, CA, USA).

4.3.6. Medulloblastoma allograft model

SMOA1 medulloblastoma model was derived from ND2:SMOA1 transgenic mice (Shanghai SLAC Laboratory Animal Co., Shanghai, China) as previously described[48]. Briefly, primary SMOA1 allografts were subcutaneously grafted into nude mice. Mice allografted with SMOA1 MB were administered compounds GDC-0449, **25** and **35** or vehicle twice a day by oral administration (*p.o.*, $n \geq 3$) once the tumor size reached $100-150$ mm^3. Tumor volumes were measured with calipers every 3 days and calculated as $0.5 \times$ length $\times$ width^2. All animal procedures were approved by Animal Care and Use Committee of Fudan University, Shanghai, China.

Acknowledgments

Author contributions

Ao Zhang, Wenfu Tan and Hongchun Liu conceived and designed the study. Xiaohua Liu performed the synthesis of the target compounds and analyzed the data. Yu Zhang, Yalei Li and Juan Wang performed the biological experiments. Huaqian Ding and Wenjing Huang assisted with carrying out experiments. Ao Zhang and Xiaohua Liu wrote the manuscript. Chunyong Ding, Wenfu Tan, Hongchun Liu and Juan Wang revised the manuscript. All the authors approved the final version of the manuscript.

Conflicts of interest

The authors have no conflicts of interest to declare.

Appendix A. Supporting information

Supporting data to this article can be found online at https://doi.org/10.1016/j.apsb.2020.07.007.

References

1. Northcott PA, Robinson GW, Kratz CP, Mabbott DJ, Pomeroy SL, Clifford SC, et al. Medulloblastoma. *Nat Rev Dis Primers* 2019;**5**:11.
2. Pui CH, Gajjar AJ, Kane JR, Qaddoumi IA, Pappo AS. Challenging issues in pediatric oncology. *Nat Rev Clin Oncol* 2011;**8**:540−9.
3. Ostrom QT, Gittleman H, Truitt G, Boscia A, Kruchko C, Barnholtz-Sloan JS. CBTRUS statistical report: primary brain and other central nervous system tumors diagnosed in the United States in 2011−2015. *Neuro Oncol* 2018;**20**:iv1−86.
4. Cavalli FMG, Remke M, Rampasek L, Peacock J, Shih DJH, Luu B, et al. Intertumoral heterogeneity within medulloblastoma subgroups. *Canc Cell* 2017;**31**:737−54.
5. Capozza MA, Trombatore G, Triarico S, Mastrangelo S, Attinà G, Maurizi P, et al. Adult medulloblastoma: an overview on current and future strategies of treatment. *Expert Opin Orphan Drugs* 2019;**7**:383−9.
6. Xin M, Ji X, de La Cruz LK, Thareja S, Wang B. Strategies to target the hedgehog signaling pathway for cancer therapy. *Med Res Rev* 2018;**38**:870−913.
7. Miranda Kuzan-Fischer C, Juraschka K, Taylor MD. Medulloblastoma in the molecular era. *J Kor Neurosurg Soc* 2018;**61**:292−301.
8. Rimkus TK, Carpenter RL, Qasem S, Chan M, Lo HW. Targeting the sonic hedgehog signaling pathway: review of smoothened and GLI inhibitors. *Cancer* 2016;**8**:22.
9. Gould SE, Low JA, Marsters Jr JC, Robarge K, Rubin LL, de Sauvage FJ, et al. Discovery and preclinical development of vismodegib. *Expet Opin Drug Discov* 2014;**9**:969−84.
10. Dlugosz A, Agrawal S, Kirkpatrick P. Vismodegib. *Nat Rev Drug Discov* 2012;**11**:437−8.
11. Pan S, Wu X, Jiang J, Gao W, Wan Y, Cheng D, et al. Discovery of NVP-LDE225, a potent and selective smoothened antagonist. *ACS Med Chem Lett* 2010;**1**:130−4.
12. Yin VT, Esmaeli B. Targeting the hedgehog pathway for locally advanced and metastatic basal cell carcinoma. *Curr Pharmaceut Des* 2017;**23**:655−9.
13. Danial C, Sarin KY, Oro AE, Chang AL. An investigator-initiated open-label trial of sonidegib in advanced basal cell carcinoma patients resistant to vismodegib. *Clin Cancer Res* 2016;**22**:1325−9.
14. Gajjar A, Stewart CF, Ellison DW, Kaste S, Kun LE, Packer RJ, et al. Phase I study of vismodegib in children with recurrent or refractory medulloblastoma: a pediatric brain tumor consortium study. *Clin Cancer Res* 2013;**19**:6305−12.
15. Robinson GW, Orr BA, Wu G, Gururangan S, Lin T, Qaddoumi I, et al. Vismodegib exerts targeted efficacy against recurrent sonic hedgehog-subgroup medulloblastoma: results from phase II pediatric brain tumor consortium studies PBTC-025B and PBTC-032. *J Clin Oncol* 2015;**33**:2646−54.
16. Li Y, Song Q, Day BW. Phase I and phase II sonidegib and vismodegib clinical trials for the treatment of paediatric and adult MB patients: a systemic review and meta-analysis. *Acta Neuropathol Commun* 2019;**7**:123.
17. Millard NE, de Braganca KC. Medulloblastoma. *J Child Neurol* 2016;**31**:1341−53.
18. Lannering B, Rutkowski S, Doz F, Pizer B, Gustafsson G, Navajas A, et al. Hyperfractioned *versus* conventional radiotherapy followed by chemotherapy in standard-risk medulloblastoma: results from the

randomized multicenter HIT-SIOP PNET 4 trial. *J Clin Oncol* 2012;**30**:3187−93.

19. Esbenshade AJ, Kocak M, Hershon L, Rousseau P, Decarie JC, Shaw S, et al. A Phase II feasibility study of oral etoposide given concurrently with radiotherapy followed by dose intensive adjuvant chemotherapy for children with newly diagnosed high-risk medulloblastoma (protocol POG 9631): a report from the Children's Oncology Group. *Pediatr Blood Cancer* 2017;**64**:e26373. 10.

20. Liu X, Ding C, Tan W, Zhang A. Medulloblastoma: molecular understanding, treatment evolution, and new developments. *Pharmacol Ther* 2020;**210**:107516.

21. Liu G, Huang W, Wang J, Liu X, Yang J, Zhang Y, et al. Discovery of novel macrocyclic hedgehog pathway inhibitors acting by suppressing the Gli-mediated transcription. *J Med Chem* 2017;**60**:8218−45.

22. Dong X, Wang C, Chen Z, Zhao W. Overcoming the resistance mechanisms of smoothened inhibitors. *Drug Discov Today* 2018;**23**: 704−10.

23. Infante P, Alfonsi R, Botta B, Mori M, Di Marcotullio L. Targeting GLI factors to inhibit the hedgehog pathway. *Trends Pharmacol Sci* 2015;**36**:547−58.

24. Villavicencio EH, Walterhouse DO, Iannaccone PM. The Sonic hedgehog-Patched-Gli pathway in human development and disease. *Am J Hum Genet* 2000;**67**:1047−54.

25. Lauth M, Bergström A, Shimokawa T, Toftgård R. Inhibition of GLI-mediated transcription and tumor cell growth by small-molecule antagonists. *Proc Natl Acad Sci U S A* 2007;**104**: 8455−60.

26. Wang J, Huang S, Tian R, Chen J, Gao H, Xie C, et al. The protective autophagy activated by GANT-61 in MYCN amplified neuroblastoma cells is mediated by PERK. *Oncotarget* 2018;**9**:14413−27.

27. Kim J, Aftab BT, Tang JY, Kim D, Lee AH, Rezaee M, et al. Itraconazole and arsenic trioxide inhibit hedgehog pathway activation and tumor growth associated with acquired resistance to smoothened antagonists. *Cancer Cell* 2013;**23**:23−34.

28. Tang Y, Gholamin S, Schubert S, Willardson MI, Lee A, Bandopadhayay P, et al. Epigenetic targeting of hedgehog pathway transcriptional output through BET bromodomain inhibition. *Nat Med* 2014;**20**:732−40.

29. Long J, Li B, Rodriguez-Blanco J, Pastori C, Volmar CH, Wahlestedt C, et al. The BET bromodomain inhibitor I-BET151 acts downstream of smoothened protein to abrogate the growth of hedgehog protein-driven cancers. *J Biol Chem* 2014;**289**:35494−502.

30. Liu Z, Wang P, Chen H, Wold EA, Tian B, et al. Drug discovery targeting bromodomain-containing protein 4. *J Med Chem* 2017;**60**: 4533−58.

31. Filippakopoulos P, Knapp S. Targeting bromodomains: epigenetic readers of lysine acetylation. *Nat Rev Drug Discov* 2014;**13**:337−56.

32. Burns CJ. Chromatin targeting: a BET inhibitor workaround. *Nat Chem Biol* 2016;**12**:469−70.

33. Henssen A, Thor T, Odersky A, Heukamp L, EI-Hindy N, Beckers A, et al. BET bromodomain protein inhibition is a therapeutic option for medulloblastoma. *Oncotarget* 2013;**4**:2080−95.

34. McDaniel KF, Wang L, Soltwedel T, Fidanze SD, Hasvold LA, Liu D, et al. Discovery of *N*-(4-(2,4-difluorophenoxy)-3-(6-methyl-7-oxo-6,7-dihydro-1*H*-pyrrolo[2,3-*c*]pyridin-4-yl)phenyl)ethanesulfonamide (ABBV-075/mivebresib), a potent and orally available bromodomain and extraterminal domain (BET) family bromodomain inhibitor. *J Med Chem* 2017;**60**:8369−84.

35. Gautam B, Johannes W, Ibrahim A, Beibei H, Minh D, Alison T, et al. First-in-human study of ABBV-075 (mivebresib), a pan-inhibitor of bromodomain and extra terminal (BET) proteins, in patients (Pts) with relapsed/refractory (RR) acute myeloid leukemia (AML): preliminary data. *J Clin Oncol* 2018;**36**:7019.

36. Bui MH, Lin X, Albert DH, Li L, Lam LT, Faivre EJ, et al. Preclinical characterization of BET family bromodomain inhibitor ABBV-075 suggests combination therapeutic strategies. *Cancer Res* 2017;**77**: 2976−89.

37. Piha-Pau SA, Sachdev JC, Barve M, LoRusso P, Szmulewitz R, Patel SP, et al. First-in-human study of mivebresib (ABBV-075), an oral pan-inhibitor of bromodomain and extra terminal proteins, in patients with pelapsed/pefractory solid tumors. *Clin Cancer Res* 2019; **25**:6309−19.

38. Faivre EJ, Wilcox D, Lin X, Hessler P, Torrent M, He W, et al. Exploitation of castration-resistant prostate cancer transcription factor dependencies by the novel BET inhibitor ABBV-075. *Mol Cancer Res* 2017;**15**:35−44.

39. Matzuk MM, McKeown MR, Filippakopoulos P, Li Q, Ma L, Agno JE, et al. Small-molecule inhibition of BRDT for male contraception. *Cell* 2012;**150**:673−84.

40. Mohammad HP, Barbash O, Creasy CL. Targeting epigenetic modifications in cancer therapy: erasing the roadmap to cancer. *Nat Med* 2019;**25**:403−18.

41. Wang L, Pratt JK, Soltwedel T, Sheppard GS, Fidanze SD, Liu D, et al. Fragment-based, structure-enabled discovery of novel pyridones and pyridone macrocycles as potent bromodomain and extra-terminal domain (BET) family bromodomain inhibitors. *J Med Chem* 2017;**60**: 3828−50.

42. Leroy J, Porhielb E, Bondonb A. Synthesis and characterization of partially *β*-fluorinated 5,10,15,20-tetraphenylporphyrins and some derivatives. *Tetrahedron* 2002;**58**:6713−22.

43. Liu G, Xue D, Yang J, Wang J, Liu X, Huang W, et al. Design, synthesis, and pharmacological evaluation of 2-(2,5-dimethyl-5,6,7,8-tetrahydroquinolin-8-yl)-*N*-aryl propanamides as novel smoothened (Smo) antagonists. *J Med Chem* 2016;**59**:11050−68.

44. Bradbury RH, Callis R, Carr GR, Chen H, Clark E, Feron L, et al. Optimization of a series of bivalent triazolopyridazine based bromodomain and extraterminal inhibitors: the discovery of (3*R*)-4-[2-[4-[1-(3-methoxy-[1,2,4]triazolo[4,3-*b*]pyridazin-6-yl)-4-piperidyl]phenoxy]ethyl]-1,3-dimethyl-piperazin-2-one (AZD5153). *J Med Chem* 2016;**59**:7801−7.

45. Wick JY. The history of benzodiazepines. *Consult Pharm* 2013;**28**: 538−48.

46. AbbVie. *A study evaluating the safety and pharmacokinetics of ABBV-075 in subjects with cancer* (ClinicalTrials.gov Identifier: NCT02391480). Available from: https://clinicaltrials.gov/ct2/show/NCT02391480 (March 18 2015).

47. Atwood SX, Sarin KY, Whitson RJ, Li JR, Kim G, Rezaee M, et al. Smoothened variants explain the majority of drug resistance in basal cell carcinoma. *Cancer Cell* 2015;**27**:342−53.

48. Hatton BA, Villavicencio EH, Tsuchiya KD, Pritchard JI, Ditzler S, Pullar B, et al. The Smo/Smo model: hedgehog-induced medulloblastoma with 90% incidence and leptomeningeal spread. *Cancer Res* 2008;**68**:1768−76.

49. Robarge KD, Brunton SA, Castanedo GM, Cui Y, Dina MS, Goldsmith R, et al. GDC-0449-a potent inhibitor of the hedgehog pathway. *Bioorg Med Chem Lett* 2009;**19**:5576−81.